# Betatron phase and coupling correction at the Cornell Electron/Positron Storage Ring

D. Sagan
*Laboratory of Nuclear Studies, Cornell University, Ithaca, New York 14853*
(Received 11 May 2000; published 26 October 2000)

The presence of quadrupole errors in a storage ring will lead to errors in the Twiss parameters and/or errors in the horizontal-vertical coupling. This in turn can lead to degradation of machine performance, such as a decrease in the luminosity. At the Cornell Electron/Positron Storage Ring, the measurement of the betatron phase along with the horizontal-vertical coupling has led to the ability to locate the position of any quadrupole errors and to calculate its strength. This is analogous to using orbit data to locate the source of a kick. Once the source of the error is known, steps can be taken to remove it or to nullify its effect.

PACS numbers: 29.20.Dh, 29.27.Fh, 29.40.Gx

## I. INTRODUCTION

The presence of quadrupole errors in a storage ring will lead to errors in the Twiss parameters and/or errors in the horizontal-vertical coupling. This in turn can lead to degradation of machine performance, such as a decrease in the luminosity. At the Cornell Electron/Positron Storage Ring (CESR), a technique for measuring the betatron phase and coupling has been developed [1] which involves shaking the beam at the horizontal and vertical betatron resonant frequencies and measuring the response at the 100 or so beam position detectors in the ring. To actually find a quadrupole error, an analysis program has been developed that can locate isolated errors from the measurement data. This analysis is analogous to the technique of using orbit data to find isolated steering kicks. The analysis is presented below for use with beta, betatron phase, and coupling data. While direct beta measurements are not currently done in standard practice at CESR, the beta analysis is given since it may be of general interest and since there is a close connection between the beta analysis and the betatron phase analysis.

## II. BETA ANALYSIS

Consider one-dimensional motion and the $2 \times 2$ transfer matrix $\mathbf{T}_{12}$ from some point $s_1$ to some point $s_2$,

$$\mathbf{T}_{12} = \begin{pmatrix} m_{11} & m_{12} \\ m_{21} & m_{22} \end{pmatrix}, \tag{1}$$

where the $m_{ij}$ are given in terms of the Twiss parameters by [2]

$$\begin{aligned} m_{11} &= \sqrt{\frac{\beta_2}{\beta_1}}\,(\cos\phi_{12} + \alpha_1 \sin\phi_{12}), \\ m_{12} &= \sqrt{\beta_1\beta_2}\,\sin\phi_{12}, \\ m_{21} &= \frac{(\alpha_1 - \alpha_2)\cos\phi_{12} - (1 + \alpha_1\alpha_2)\sin\phi_{12}}{\sqrt{\beta_1\beta_2}}, \\ m_{22} &= \sqrt{\frac{\beta_1}{\beta_2}}\,(\cos\phi_{12} - \alpha_2 \sin\phi_{12}), \end{aligned} \tag{2}$$

with $\phi_{12}$ being the phase advance from $s_1$ to $s_2$. By using Eq. (2), $\beta_2$ can be written in terms of the Twiss parameters at $s_1$ via

$$\beta_2 = m_{11}^2\beta_1 - 2m_{11}m_{12}\alpha_1 + m_{12}^2\gamma_1, \tag{3}$$

where the following relation has been used:

$$\beta\gamma = 1 + \alpha^2. \tag{4}$$

It will be assumed that the strength of any quadrupole error is small so that terms that are second order in the perturbation can be ignored. Assume for the moment that there are no quadrupole errors between $s_1$ and $s_2$ so the $m_{ij}$ are constant. In this case, the variation of $\beta_2$ due to any quadrupole errors is given from Eq. (3) to be

$$\delta\beta_2 = m_{11}^2\delta\beta_1 - 2m_{11}m_{12}\delta\alpha_1 + m_{12}^2\delta\gamma_1. \tag{5}$$

Here, and in all equations below, $m_{ij}$, $\beta$, $\phi$, etc., refer to the unperturbed values and $\delta\beta$, $\delta\alpha$, and $\delta\gamma$, etc., are the variation from the unperturbed values due to any quadrupole errors. Using Eqs. (2) and (4) in Eq. (5) shows that, in a region where there are no quadrupole errors, $\delta\beta$ can be written in the form

$$\frac{\delta\beta(s)}{\beta(s)} = \lambda\,\sin 2\phi(s) + \rho\,\cos 2\phi(s), \tag{6}$$

where $\lambda$ and $\rho$ are constants. A "free beta wave" thus oscillates as $2\phi(s)$—at twice the frequency of an orbit wave.

For the purposes of this analysis, a quadrupole error will be modeled as having zero length. If the error has zero strength, the transfer matrix across the error is just the unit matrix

$$\begin{pmatrix} m_{11} & m_{12} \\ m_{21} & m_{22} \end{pmatrix} = \begin{pmatrix} 1 & 0 \\ 0 & 1 \end{pmatrix}. \tag{7}$$

If $s_1$ is taken to be just before the error, and $s_2$ is taken to be just after the error, then using this with Eq. (2) gives

$$\alpha_2 = \alpha_1, \quad \beta_2 = \beta_1, \quad \text{and} \quad \phi_{12} = 0. \tag{8}$$

If the error has a nonzero strength of $\delta kl$, the perturbation of the transfer matrix across the error is

  

$$\begin{pmatrix} \delta m_{11} & \delta m_{12} \\ \delta m_{21} & \delta m_{22} \end{pmatrix} = \begin{pmatrix} 0 & 0 \\ \delta kl & 0 \end{pmatrix}, \tag{9}$$

with the convention here that a positive $\delta k$ represents a defocusing perturbation. Using Eqs. (2) and (8) in Eq. (9) gives

$$\delta\alpha_2 = \delta\alpha_1 - \beta_1 \delta kl, \quad \delta\beta_2 = \delta\beta_1, \quad \delta\phi_{12} = 0. \tag{10}$$

Given a quadrupole error at some point $s_0$, it is assumed that the perturbation is "isolated" so that it is the only error in some local region. From Eq. (6), the general solution in this local region is

$$\frac{\delta\beta(s)}{\beta(s)} = \begin{cases} \lambda_a \sin 2\phi(s) + \rho_a \cos 2\phi(s), & s < s_0, \\ \lambda_b \sin 2\phi(s) + \rho_b \cos 2\phi(s), & s > s_0, \end{cases} \tag{11}$$

where $\lambda_a$, $\rho_a$, $\lambda_b$, and $\rho_b$ are constants. Since the problem has been linearized by using first-order perturbation theory, the general solution $\delta\beta(s)$ is the sum of a homogeneous part $\delta\beta_h$ plus an inhomogeneous part $\delta\beta_i$,

$$\delta\beta(s) = \delta\beta_h(s) + \delta\beta_i(s). \tag{12}$$

The homogeneous part is the solution when there is no error present and is of the form given by Eq. (6). The inhomogeneous part is the solution with the error and with a boundary condition which we are free to choose. The boundary condition will be chosen so that $\delta\beta_i(s) = 0$ for $s < s_0$. From Eqs. (6) and (10), along with the relations $2\alpha = -d\beta/ds$ and $d\phi/ds = 1/\beta$, the inhomogeneous solution is

$$\frac{\delta\beta_i(s)}{\beta(s)} = \begin{cases} 0, & s < s_0, \\ \delta kl \sin[2(\phi(s) - \phi_0)], & s > s_0, \end{cases} \tag{13}$$

where $\phi_0 \equiv \phi(s_0)$ is the phase at the error. The procedure for locating a quadrupole error is as follows: Given a putative location for an error, a region labeled "*a*" is chosen that is just before this location and a region labeled "*b*" is chosen that is just after the location, as shown in Fig. 1. By using Eq. (11) and the $\delta\beta$ data in the *a* region, a linear least squares fit is used to determine $\lambda_a$ and $\rho_a$. Similarly, $\lambda_b$ and $\rho_b$ are obtained from a linear least squares fit to the data from the *b* region. The inhomogeneous part of the fit is now obtained by subtracting out the homogeneous part of Eq. (11) to give

$$\frac{\delta\beta_i(s)}{\beta(s)} = \begin{cases} 0, & s < s_0, \\ \lambda_{ba} \sin 2\phi(s) + \rho_{ba} \cos 2\phi(s), & s > s_0, \end{cases} \tag{14}$$

where

$$\lambda_{ba} = \lambda_b - \lambda_a \quad \text{and} \quad \rho_{ba} = \rho_b - \rho_a. \tag{15}$$

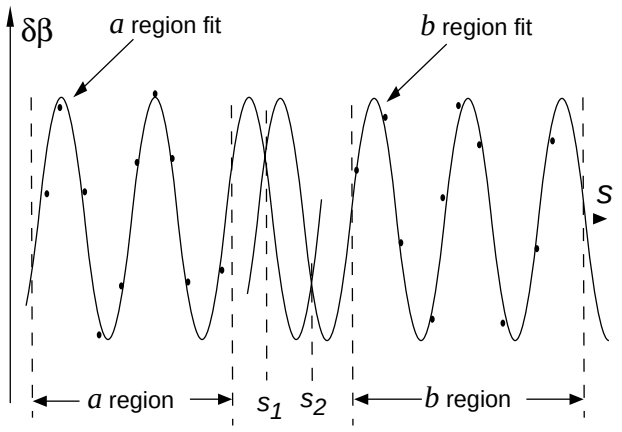


FIG. 1. Schematic diagram of the analysis to find a quadrupole error using a $\beta$ measurement. Fits to $\delta\beta$ in regions *a* and *b* give sinusoidal-like "free waves." Pictorially, the possible error locations (labeled $s_1$ and $s_2$ in this example) can be found by extending the two fits into the region between *a* and *b*. The error locations are where the fits cross.

The phase at the error is found by comparing Eq. (13) with Eq. (14),

$$\tan 2\phi_0 = -\frac{\rho_{ba}}{\lambda_{ba}}. \tag{16}$$

The magnitude of the error is also found by comparing Eq. (13) with Eq. (14),

$$\delta kl = \lambda_{ba} \cos 2\phi_0 - \rho_{ba} \sin 2\phi_0 = \pm A_\beta, \tag{17}$$

where the amplitude $A_\beta$ is defined by

$$A_\beta^2 \equiv \lambda_{ba}^2 + \rho_{ba}^2. \tag{18}$$

The solutions to Eq. (16) are a series of points spaced $\pi/2$ apart in phase with the restriction that $\phi_0$ corresponds to a location somewhere between the *a* and *b* regions (cf. Fig. 1). The magnitude of $\delta k$ is the same for all solutions, but the sign of $\delta k$ for consecutive solutions is opposite.

To determine how well the calculation has fit the data, a figure of merit can be defined as follows: Considering the *a* region first, the variance $\sigma_a$ between the data and the fit is

$$\sigma_a^2 \equiv \frac{1}{N_a} \sum_{j \in a} [\delta\beta_j(\text{data}) - \delta\beta_j(\text{fit})]^2, \tag{19}$$

where $N_a$ is the number of data points and the sum is over all points in the *a* region. The uncertainty $\sigma_{\lambda a}$ in $\lambda_a$ is then given by [3]

$$\sigma_{\lambda a}^2 = \sigma_a^2 \sum_{j \in a} \left( \frac{\partial \lambda_a}{\partial(\delta\beta_j)} \right)^2, \tag{20}$$

with a similar equation for the uncertainty $\sigma_{\rho a}$ in $\rho_a$. The calculation of the goodness-of-fit for the *b* region is handled in a similar fashion. The relative uncertainty in the kick $\sigma_{\delta k}/\delta k$ is obtained from Eqs. (17) and (18),

$$\frac{\sigma_{\delta k}}{\delta k} = \frac{\sqrt{\lambda_{ba}^2\sigma_{\lambda ba}^2 + \rho_{ba}^2\sigma_{\rho ba}^2}}{A_\beta^2}, \tag{21}$$

where $\sigma_{\lambda ba}$ and $\sigma_{\rho ba}$ are computed from Eq. (15):

$$\sigma_{\lambda ba}^2 = \sigma_{\lambda a}^2 + \sigma_{\lambda b}^2 \quad \text{and} \quad \sigma_{\rho ba}^2 = \sigma_{\rho a}^2 + \sigma_{\rho b}^2 . \tag{22}$$

Similarly, the uncertainty $\sigma_\phi$ in $\phi_0$ is obtained from Eq. (16) to be

$$\sigma_\phi = \frac{\sqrt{\rho_{ba}^2\sigma_{\lambda ba}^2 + \lambda_{ba}^2\sigma_{\rho ba}^2}}{2A_\beta^2} . \tag{23}$$

The necessary (but not sufficient) conditions that the calculation is accurate are

$$\frac{\sigma_{\delta k}}{\delta k} \ll 1 \quad \text{and} \quad \sigma_\phi \ll 1 . \tag{24}$$

## III. PHASE ANALYSIS

The betatron phase $\phi$ is related to $\beta$ by the standard equation

$$\frac{d\phi}{ds} = \frac{1}{\beta} . \tag{25}$$

Taking the variation of both sides gives

$$\frac{d\delta\phi}{d\phi} = \frac{-\delta\beta}{\beta} . \tag{26}$$

The analysis of $\delta\phi$ is thus obtained from the $\delta\beta$ analysis via a simple integration. In a region without quadrupole errors, $\delta\phi$ is obtained by integrating Eq. (6),

$$\delta\phi(s) = \xi \sin 2\phi(s) + \eta \cos 2\phi(s) + C , \tag{27}$$

where $\xi$, $\eta$, and $C$ are constants. A free phase wave looks similar to a free beta wave but with an offset. For a region where there is an isolated quadrupole error at $s_0$ the general solution is obtained from Eq. (27),

$$\delta\phi(s) = \begin{cases} \xi_a \sin 2\phi(s) + \eta_a \cos 2\phi(s) + C_a, & s < s_0 , \\ \xi_b \sin 2\phi(s) + \eta_b \cos 2\phi(s) + C_b, & s > s_0 . \end{cases} \tag{28}$$

Integrating Eq. (13) gives the inhomogeneous part of the solution with the boundary condition $\delta\phi_i(s) = 0$ for $s < s_0$,

$$\delta\phi_i(s) = \begin{cases} 0, & s < s_0 , \\ \frac{\beta_0\delta kl}{2}[\cos 2(\phi(s) - \phi_0) - 1], & s > s_0 . \end{cases} \tag{29}$$

This is to be compared to the inhomogeneous part of Eq. (28),

$$\delta\phi_i(s) = \begin{cases} 0, & s < s_0 , \\ \xi_{ba} \sin 2\phi(s) + \eta_{ba} \cos 2\phi(s) + C_{ba}, & s > s_0 , \end{cases} \tag{30}$$

where

$$\xi_{ba} = \xi_b - \xi_a, \quad \eta_{ba} = \eta_b - \eta_a, \quad C_{ba} = C_b - C_a . \tag{31}$$

Like the beta analysis, regions $a$ and $b$ are chosen to bracket a possible quadrupole error (cf. Fig. 1). $\xi_a$, $\eta_a$, and $C_a$ along with $\xi_b$, $\eta_b$, and $C_b$ are computed via a linear least squares fit of Eq. (28) to the data in the two regions. Comparing Eq. (29) with Eq. (30), the fitted parameters should obey the relationship

$$|C_{ba}| = A_\phi , \tag{32}$$

where

$$A_\phi^2 \equiv \xi_{ba}^2 + \eta_{ba}^2 . \tag{33}$$

Equation (32) is the condition needed so that $\delta\phi(s)$ is continuous and has a continuous derivative at $s_0$, as shown in Fig. 2(a). In actuality, measurement errors and/or the presence of additional quadrupole errors in the region will typically lead to the situations shown in Figs. 2(b) or 2(c), where the fits do not intersect or they intersect with a discontinuous derivative. The best solution is to choose, for $s_0$, the point(s) where the derivatives match and any discontinuity is smaller than $A_\phi/2$, as shown in Fig. 2. Using this criterion with Eqs. (29) and (30) gives for $\phi_0$

$$\sin 2\phi_0 = \frac{-\xi_{ba}\,\mathrm{sgn}C_{ba}}{A_\phi}, \qquad \cos 2\phi_0 = \frac{-\eta_{ba}\,\mathrm{sgn}C_{ba}}{A_\phi}, \tag{34}$$

where

$$\mathrm{sgn}C_{ba} \equiv \begin{cases} 1, & C_{ba} > 0 , \\ -1, & C_{ba} < 0 . \end{cases} \tag{35}$$

Comparing Eq. (29) with Eq. (30) gives two equations for the magnitude of the error

$$\beta_0\delta kl = -2C_{ba} , \tag{36}$$

and

$$\beta_0\delta kl = 2(\xi_{ba} \sin 2\phi_0 + \eta_{ba} \cos 2\phi_0) . \tag{37}$$

Since Eq. (32) is not obeyed in practice, the right-hand side of Eqs. (36) and (37) will not give the same result. A good compromise is to take the average of the two equations and compute $\delta k$ via

$$\beta_0\delta kl = \xi_{ba} \sin 2\phi_0 + \eta_{ba} \cos 2\phi_0 - C_{ba} . \tag{38}$$

As opposed to the beta analysis, Eqs. (34) have solutions spaced $\pi$ apart, and all solutions have the same sign for the strength of the error.

The calculation of the uncertainty in the strength and location of the perturbation is analogous to that of the

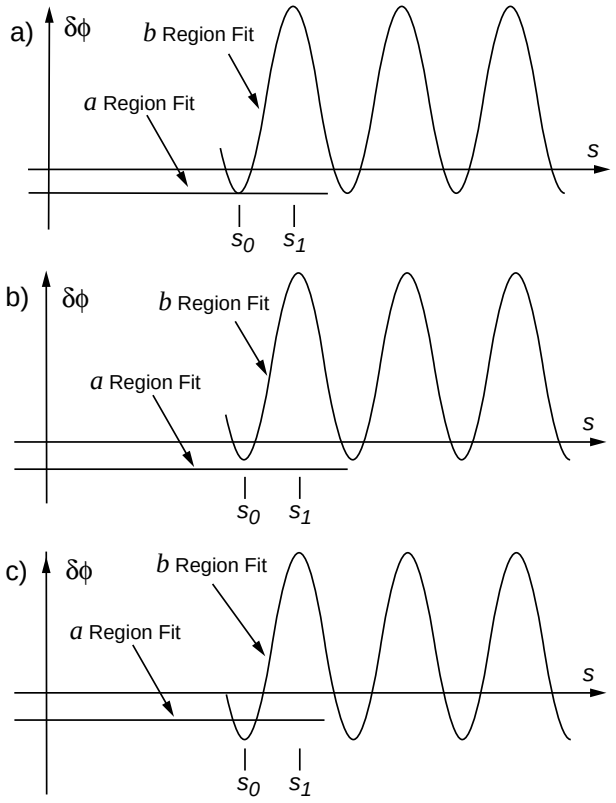


FIG. 2. In theory, the $a$ and $b$ region fits of $\delta\phi(s)$ are continuous and have a continuous derivative at $s_0$, as shown in (a). (For simplicity, the $a$ region fit is taken here to be a straight line.) In practice the fits to the $a$ and $b$ regions may (b) fail to intersect or (c) intersect with a discontinuous derivative. The best guess for the location of the error (labeled $s_0$) is where the derivatives match and where any discontinuity is smaller than $A_\phi/2$ (so that the point labeled $s_1$ is rejected as a possible location for the error).

previous section. The relative uncertainty of the strength is

$$\frac{\sigma_{\delta k}}{\delta k} = \frac{\sqrt{\xi_{ba}^2\sigma_{\xi ba}^2 + \eta_{ba}^2\sigma_{\eta ba}^2 + C_{ba}^2\sigma_{Cba}^2}}{|\xi_{ba}\sin 2\phi_0 + \eta_{ba}\cos 2\phi_0 - C_{ba}|^2}, \tag{39}$$

where, from Eq. (31),

$$\sigma_{\xi ba}^2 = \sigma_{\xi b}^2 + \sigma_{\xi a}^2, \qquad \sigma_{\eta ba}^2 = \sigma_{\eta b}^2 + \sigma_{\eta a}^2, \qquad \sigma_{Cba}^2 = \sigma_{Cb}^2 + \sigma_{Ca}^2, \tag{40}$$

with

$$\sigma_{\xi a} = \sigma_a^2 \sum_{j\in a}\left(\frac{\partial \xi_a}{\partial(\delta\phi_j)}\right)^2, \tag{41}$$

and similar equations for $\sigma_{\xi b}$, etc. Finally $\sigma_a$ and $\sigma_b$ are computed in analogy to Eq. (19),

$$\sigma_a^2 \equiv \frac{1}{N_a}\sum_{j\in a}[\delta\phi_j(\text{data}) - \delta\phi_j(\text{fit})]^2, \tag{42}$$

with a similar equation for $\sigma_b$. The uncertainty $\sigma_\phi$ in $\phi_0$ is analogous to Eq. (23),

$$\sigma_\phi = \frac{\sqrt{\xi_{ba}^2\sigma_{\eta ba}^2 + \eta_{ba}^2\sigma_{\xi ba}^2}}{2A_\phi}. \tag{43}$$

The conditions needed for an accurate calculation are given by Eqs. (24).

An additional figure of merit can be obtained by noting that even if $\sigma_{\delta k}/\delta k$ and $\sigma_\phi$ are small, the results of the calculation may not mean much if there are multiple quadrupole errors between the fitted regions. Since multiple errors will tend to make $|C_{ba}|$ and $A_\phi$ different [cf. Eq. (32)], a figure of merit $\chi_C$ may be defined by

$$\chi_C \equiv \frac{|C_{ba}| - A_\phi}{|C_{ba}| + A_\phi}. \tag{44}$$

A necessary (but not sufficient) condition necessary for the analysis to be valid is

$$|\chi_C| \ll 1. \tag{45}$$

Figure 3 shows an example of the phase analysis. The data shown in the figure were obtained after conditions in the CESR ring suddenly deteriorated and a phase measurement was taken in order to try to diagnose the problem. Here $\delta\phi$ is the difference between the measured phase and the theoretical design phase. Figure 3(a) shows the measured $\delta\phi$ for the vertical mode along with the chosen $a$ and $b$ fit regions. Figure 3(b) shows the $\delta\phi$ data with the $a$ region fit subtracted off. By subtracting off the $a$ region fit, Fig. 3(b) is displaying the inhomogeneous part of $\delta\phi$

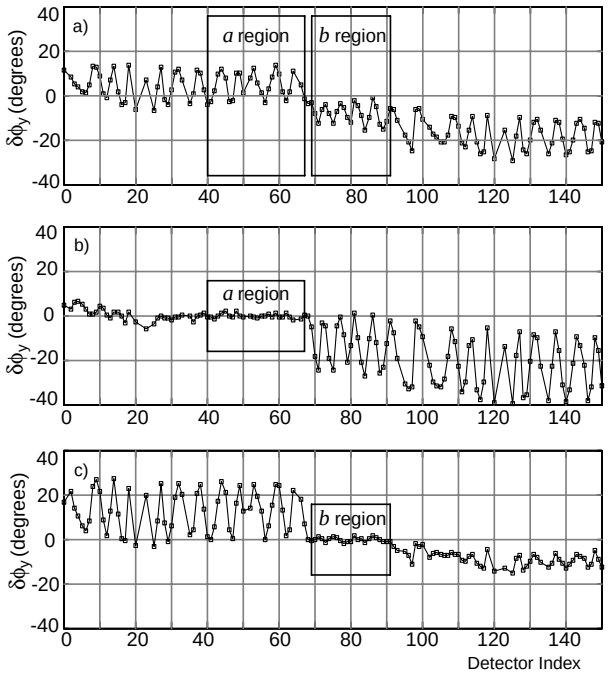


FIG. 3. Analysis of vertical phase data. $\delta\phi$ is the difference between the measured and theoretical design phase. (a) $\delta\phi$ as obtained from a measurement, (b) $\delta\phi$ with the fit from the $a$ region subtracted off, (c) $\delta\phi$ with the fit from the $b$ region subtracted off. The boxes shown in the figures correspond to the fit regions.

[cf. Eq. (30)]. Figure 3(c) shows the $\delta\phi$ data with the $b$ region fit subtracted off; that is, Fig. 3(c) shows the inhomogeneous part of $\delta\phi$ but with a boundary condition of $\delta\phi(s) = 0$ for $s > s_0$. Figures 3(b) and 3(c) clearly show the general location of the quadrupole error which is indicated by where the flat and oscillatory parts of the curves meet. The boundaries of the fit regions were adjusted by hand in an iterative process so that the region between the fit regions was small enough so that there was only one unambiguous solution. As a help in adjusting the boundary regions, figures of merit $\chi_a$ and $\chi_b$ for the individual fits may be defined. For the $a$ region,

$$\chi_a \equiv \frac{\sigma_a}{\sqrt{\xi_a^2 + \eta_a^2}}, \tag{46}$$

with a similar definition for the $b$ region. The fits are good if $\chi_a \ll 1$ and $\chi_b \ll 1$. The region boundaries are adjusted with an eye to maintain $\chi_a$ and $\chi_b$ small. In the present example, $\chi_a$ and $\chi_b$ were 0.07 and 0.09, respectively, indicating a good fit. $\chi_C$ was calculated to be 0.006, so the measured data was well fit with the single error model. $\sigma_\phi$ was calculated from Eq. (43) to be 0.035 rad (2°) which, using Eq. (25), and with a $\beta_y$ in the region of 30 m, translated to an uncertainty in the location of the error of about $\pm 1$ m. In this particular case the calculated location of the error was at a particular quadrupole magnet. The controller circuit board for this quadrupole was replaced and the problem was fixed. A subsequent phase measurement showed no significant phase errors.

The horizontal axis in Fig. 3 is the detector index. In CESR, the beam detectors are labeled, starting at the interaction point, from 0 to 99. Since a quadrupole error may be near the interaction point, in order to ensure that it is always possible to choose fit regions on both sides of any location, the plots are extended past detector 99 to include an additional $1/2$ of the ring; that is, for example, the detector labeled 132 in the figure is actually detector 32 (=132 − 100). The formula needed to extend the data past the interaction point to detector $j + 100$ is

$$\delta\phi(j + 100) = \delta\phi(j) + \delta\phi_{\text{ring}}, \tag{47}$$

where $\delta\phi_{\text{ring}}$ in this case is the difference in tune between the measured data and the tune as calculated from the theoretical design lattice.

## IV. COUPLING ANALYSIS

Horizontal-vertical coupling may be parametrized using the $2 \times 2$ $\overline{\mathbf{C}}$ matrix [4]. The $\overline{\mathbf{C}}$ matrix is obtained via a similarity transformation of the one-turn $4 \times 4$ transfer matrix $\mathbf{T}$ into normal mode form

$$\mathbf{T} = \mathbf{V}\mathbf{U}\mathbf{V}^{-1}, \tag{48}$$

where the normal mode matrix $\mathbf{U}$ is of the form

$$\mathbf{U} = \begin{pmatrix} \mathbf{A} & \mathbf{0} \\ \mathbf{0} & \mathbf{B} \end{pmatrix}, \tag{49}$$

and $\mathbf{V}$ is of the form

$$\mathbf{V} = \begin{pmatrix} \gamma\mathbf{I} & \mathbf{C} \\ -\mathbf{C}^{+} & \gamma\mathbf{I} \end{pmatrix}, \tag{50}$$

with "+" denoting the symplectic conjugate. Since $\mathbf{V}$ is required to be symplectic, $\gamma$ and $\mathbf{C}$ are related by

$$\gamma^2 + ||\mathbf{C}|| = 1. \tag{51}$$

$\mathbf{C}(s)$ is a measure of the local coupling; if $\mathbf{C} = 0$, then $\mathbf{V} = 1$ and using this in Eqs. (48) and (49) shows that $\mathbf{T}$ is decoupled. Instead of working with $\mathbf{C}$, though, it is convenient to remove factors of $\beta$ and work with the normalized matrix $\overline{\mathbf{C}}$ given by

$$\overline{\mathbf{C}} = \mathbf{G}_a \mathbf{C} \mathbf{G}_b^{-1}, \tag{52}$$

where $\mathbf{G}_a$ and $\mathbf{G}_b$ are normalization matrices for the $a$ and $b$ normal modes respectively given by

$$\mathbf{G}_a = \begin{pmatrix} \frac{1}{\sqrt{\beta_a}} & 0 \\ \frac{\alpha_a}{\sqrt{\beta_a}} & \sqrt{\beta_a} \end{pmatrix}, \tag{53}$$

with a similar equation for $\mathbf{G}_b$. The Twiss parameters $\beta_a$, etc., are obtained from the eigenmode $\mathbf{A}$ and $\mathbf{B}$ matrices which can be written in the standard form

$$\mathbf{A} = \begin{pmatrix} \cos\theta_a + \alpha_a \sin\theta_a & \beta_a \sin\theta_a \\ -\gamma_a \sin\theta_a & \cos\theta_a - \alpha_a \sin\theta_a \end{pmatrix}, \tag{54}$$

with a similar equation for $\mathbf{B}$. The physical interpretation of the $\overline{\mathbf{C}}$ matrix is that for excitation of the horizontal-like normal mode the $\overline{C}_{22}$ component is a measure of the vertical motion that is in phase with the horizontal motion while the $\overline{C}_{12}$ component is a measure of the out-of-phase part of the vertical motion. For the excitation of the vertical-like normal mode, $\overline{C}_{11}$ gives the in-phase component and $\overline{C}_{12}$ gives the out-of-phase component of the horizontal motion with respect to the vertical motion [1].

As in the beta and phase analysis, we need to know how the $\overline{\mathbf{C}}$ matrix behaves in a coupler free region and how $\overline{\mathbf{C}}$ changes across a coupler. It is shown in the Appendix that, in a coupler free region, $\overline{\mathbf{C}}$ behaves as

$$\overline{\mathbf{C}}(s) = s\mathbf{S}(\phi_c - \phi_+(s)) + r\,\mathbf{R}(\theta_c + \phi_-(s)), \tag{55}$$

where $s$, $\phi_c$, $r$, and $\theta_c$ are constants, $\mathbf{R}$ and $\mathbf{S}$ are rotation and antirotation matrices given by Eqs. (A7) and (A9), and the sum and difference phases $\phi_+$ and $\phi_-$ are given by Eq. (A11). It is assumed that any coupling is small so first order perturbation theory can be used. To first order in the coupling (that is, to first order in the components of $\mathbf{C}$ or $\overline{\mathbf{C}}$), Eq. (51) gives

$$\gamma = 1. \tag{56}$$

Using this and Eqs. (48), (49), and (50) gives

$$\mathbf{T} = \begin{pmatrix} \mathbf{A} & \mathbf{CB} - \mathbf{AC} \\ \mathbf{BC}^{+} - \mathbf{C}^{+}\mathbf{A} & \mathbf{B} \end{pmatrix}. \tag{57}$$

Equation (57) shows that, to first order, the on-diagonal $2 \times 2$ submatrices of $\mathbf{T}$ are unaffected by the coupling. Thus, the eigenmode Twiss parameters are unaffected [cf. Eq. (54)] so that $\beta_a = \beta_x$, $\phi_a = \phi_x$, etc., where $\beta_x$, $\phi_x$, etc., are the Twiss parameters as calculated without any coupling.

For the present analysis, coupling errors are modeled as thin skew quadrupoles. The $4 \times 4$ transfer matrix $\mathbf{T}_c$ for a coupler is then

$$\mathbf{T}_c = \begin{pmatrix} \mathbf{1} & -\mathbf{q} \\ -\mathbf{q} & \mathbf{1} \end{pmatrix}, \tag{58}$$

where

$$\mathbf{q} = \begin{pmatrix} 0 & 0 \\ \delta q & 0 \end{pmatrix}, \tag{59}$$

with $\delta q$ being the strength of the coupler. The sign has been chosen here so that an upright quadrupole with a positive $k$ (horizontally focusing) that is rotated by $+45°$ will have a transfer matrix like Eq. (58) with a positive $\delta q$. The one-turn matrix $\mathbf{T}_2$, located at a point just after a coupler, is related to the one-turn matrix $\mathbf{T}_1$, located at a point just before the coupler, via

$$\mathbf{T}_2 = \mathbf{T}_c \mathbf{T}_1 \mathbf{T}_c^{-1}. \tag{60}$$

Using Eqs. (57) and (58) in Eq. (60), and comparing with Eq. (57), gives, to first order, and with the help of Eq. (52),

$$\overline{\mathbf{C}}_2 = \overline{\mathbf{C}}_1 - \overline{\mathbf{q}}, \tag{61}$$

where

$$\overline{\mathbf{q}} = \begin{pmatrix} 0 & 0 \\ \delta \overline{q} & 0 \end{pmatrix}, \tag{62}$$

with

$$\delta \overline{q} = \sqrt{\beta_a \beta_b}\, \delta q\,. \tag{63}$$

The coupling measurement at CESR can measure the $\overline{C}_{11}$, $\overline{C}_{12}$, and $\overline{C}_{22}$ components of $\overline{\mathbf{C}}$. For various technical reasons, the errors in the $\overline{C}_{12}$ data are less than the errors present in the measurement of the other components [1]. Therefore, the following analysis will consider only the $\overline{C}_{12}$ component. Extending the analysis to the other components is a trivial matter. From Eqs. (55), (A7), and (A9), the general solution for $\overline{C}_{12}$ in a region with a single coupler at $s_0$ is

$$\overline{C}_{12}(s) = \begin{cases} \tau_a \sin\phi_-(s) + \mu_a \cos\phi_-(s) + \lambda_a \sin\phi_+(s) + \rho_a \cos\phi_+(s), & s < s_0\,, \\ \tau_b \sin\phi_-(s) + \mu_b \cos\phi_-(s) + \lambda_b \sin\phi_+(s) + \rho_b \cos\phi_+(s), & s > s_0\,, \end{cases} \tag{64}$$

where $\tau$, $\mu$, $\lambda$, and $\rho$ are constants. The inhomogeneous part of the solution will be chosen with a boundary condition such that $\overline{\mathbf{C}}_i(s) = 0$. From Eqs. (55) and (61), the inhomogeneous solution is

$$\overline{\mathbf{C}}_i(s) = \begin{cases} 0, & s < s_0\,, \\ \frac{\delta \overline{q}}{2}\{\mathbf{R}[\frac{\pi}{2} + \phi_-(s) - \phi_-(s_0)] - \mathbf{S}[\frac{\pi}{2} - \phi_+(s) + \phi_+(s_0)]\}, & s > s_0\,. \end{cases} \tag{65}$$

For the $\overline{C}_{12}$ component, Eq. (65) becomes

$$\overline{C}_{i,12}(s) = \begin{cases} 0, & s < s_0\,, \\ \frac{\delta \overline{q}}{2}\{\cos[\phi_-(s) - \phi_-(s_0)] - \cos[\phi_+(s) - \phi_+(s_0)]\}, & s > s_0\,. \end{cases} \tag{66}$$

This is to be compared to the inhomogeneous part of Eq. (64), which is

$$\overline{C}_{i,12}(s) = \begin{cases} 0, & s < s_0\,, \\ \tau_{ba} \sin\phi_-(s) + \mu_{ba} \cos\phi_-(s) + \lambda_{ba} \sin\phi_+(s) + \rho_{ba} \cos\phi_+(s), & s > s_0\,, \end{cases} \tag{67}$$

where

$$\begin{aligned} \tau_{ba} &= \tau_b - \tau_a, \qquad \mu_{ba} = \mu_b - \mu_a\,, \\ \lambda_{ba} &= \lambda_b - \lambda_a, \qquad \rho_{ba} = \rho_b - \rho_a\,. \end{aligned} \tag{68}$$

As with the beta and phase analysis, given a putative coupler location $s_0$, two regions labeled $a$ and $b$ are chosen on either side. Using the data from the $a$ region, a least squares fit can be used to determine $\tau_a$, $\mu_a$, $\lambda_a$, and $\rho_a$. Similarly, $\tau_b$, $\mu_b$, $\lambda_b$, and $\rho_b$ are obtained from a least squares fit using the data from the $b$ region. The phase at the coupler is found by comparing Eq. (66) with Eq. (67),

$$\tan\phi_+(s_0) = \frac{\lambda_{ba}}{\rho_{ba}}\,, \tag{69}$$

and

$$\tan\phi_-(s_0) = \frac{\tau_{ba}}{\mu_{ba}}\,. \tag{70}$$

There are multiple solutions to Eqs. (69) and (70) spaced $\pi$ apart in $\phi_+$ and $\phi_-$, respectively. Since both $\phi_+$ and $\phi_-$ are known functions of $s$, they will individually give values for $s_0$. A valid solution must have these two values for $s_0$ agree within the experimental error.

The strength of the coupler is given by comparing Eq. (66) to Eq. (67),

$$\frac{\delta \overline{q}}{2} = -\lambda_{ba} \sin\phi_+(s_0) - \rho_{ba} \cos\phi_+(s_0)\,, \tag{71}$$

and

$$\frac{\delta \overline{q}}{2} = \tau_{ba} \sin\phi_-(s_0) + \mu_{ba} \cos\phi_-(s_0)\,. \tag{72}$$

Amplitudes $A_+$ and $A_-$ may be defined by

$$A_+^2 \equiv \lambda_{ba}^2 + \rho_{ba}^2 \quad \text{and} \quad A_-^2 \equiv \tau_{ba}^2 + \mu_{ba}^2 . \tag{73}$$

Using this, Eqs. (71) may be put in a more transparent form,

$$|\delta\overline{q}| = 2A_+ = 2A_- . \tag{74}$$

The disadvantage of Eqs. (74) is that the sign of $\delta\overline{q}$ is lost.

The relative uncertainty of the strength of the coupler is computed from Eqs. (71) and (72),

$$\begin{aligned} \frac{\sigma_{\delta q+}}{\delta q} &= \frac{\sqrt{\lambda_{ba}^2\sigma_{\lambda ba}^2 + \rho_{ba}^2\sigma_{\rho ba}^2}}{A_+} , \\ \frac{\sigma_{\delta q-}}{\delta q} &= \frac{\sqrt{\tau_{ba}^2\sigma_{\tau ba}^2 + \mu_{ba}^2\sigma_{\mu ba}^2}}{A_-} , \end{aligned} \tag{75}$$

where $\sigma_{\delta q+}$ is the uncertainty in $\delta\overline{q}$ from using Eq. (71), and $\sigma_{\delta q-}$ is the uncertainty in $\delta\overline{q}$ from using Eq. (72). The uncertainty in the phase at the kick is computed from Eqs. (69) and (70),

$$\begin{aligned} \sigma_{\phi+} &= \frac{\sqrt{\rho_{ba}^2\sigma_{\lambda ba}^2 + \lambda_{ba}^2\sigma_{\rho ba}^2}}{A_+} , \\ \sigma_{\phi-} &= \frac{\sqrt{\mu_{ba}^2\sigma_{\tau ba}^2 + \tau_{ba}^2\sigma_{\mu ba}^2}}{A_-} , \end{aligned} \tag{76}$$

where $\sigma_{\phi+}$ and $\sigma_{\phi-}$ are the uncertainties in $\phi_+(s_0)$ and $\phi_-(s_0)$, respectively. $\sigma_{\lambda ba}$, $\sigma_{\rho ba}$, etc., are computed in an analogous fashion to the computations in the previous sections [cf. Eq. (22)].

It is possible for the data to be such that there is a poor fit to $\tau$ and $\mu$ while the fit for $\lambda$ and $\rho$ is quite good. This is true since the variation of $\phi_-(s)$ as a function of $s$ can be small compared to the variation of $\phi_+(s)$, and a fit will tend to be poor if the phase advance across the fitting region is small. Fortunately, since $\lambda$ and $\rho$ alone will give the strength and location of a coupler, this is not a serious drawback.

Figure 4 shows an analysis of $\overline{C}_{12}$ data. Figure 4(a) shows the $\overline{C}_{12}$ data along with the chosen $a$ and $b$ fit regions. Analogous to Fig. 3, Figs. 4(b) and 4(c) show the $\overline{C}_{12}$ data with the $a$ and $b$ fits subtracted off, respectively. The fit regions were adjusted by hand with the purpose of identifying the coupling source near detector 63. As a help in adjusting the boundary regions, figures of merit $\chi_+$ and $\chi_-$ for the fits to $\tau$ and $\mu$, and for $\lambda$ and $\rho$, may be defined. For the $a$ region

$$\chi_{a+} \equiv \sqrt{\frac{\sigma_{\lambda a}^2 + \sigma_{\rho a}^2}{\lambda_a^2 + \rho_a^2}} , \qquad \chi_{a-} \equiv \sqrt{\frac{\sigma_{\tau a}^2 + \sigma_{\mu a}^2}{\tau_a^2 + \mu_a^2}} , \tag{77}$$

with $\chi_{b+}$ and $\chi_{b-}$ defined for the $b$ region fit in an analogous manner. In this particular case, $\chi_{a+} = 0.08$, $\chi_{a-} = 0.17$, $\chi_{b+} = 0.05$, and $\chi_{b-} = 0.06$. These values show

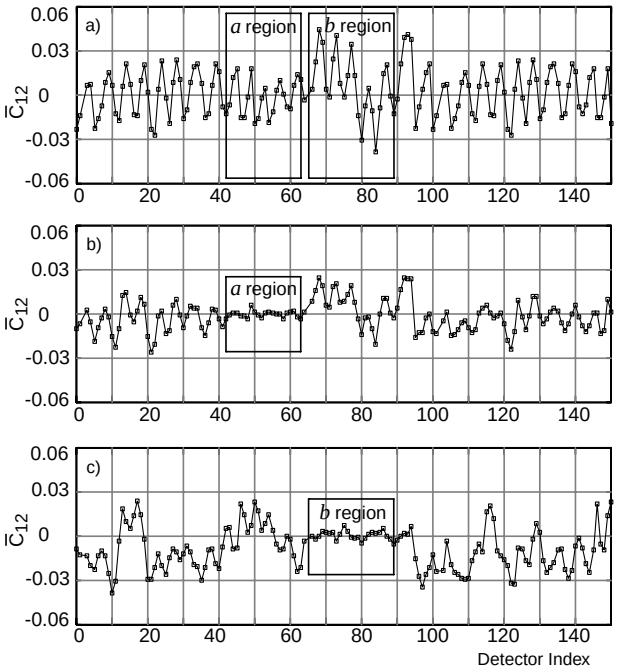


FIG. 4. Analysis of $\overline{C}_{12}$ data. (a) $\overline{C}_{12}$ data, (b) $\overline{C}_{12}$ data with the $a$ region fit subtracted off, (c) $\overline{C}_{12}$ data with the $b$ region fit subtracted off. The boxes shown in the figures correspond to the fit regions.

that there is a good match between the data and the fit. The phase errors were $\sigma_{\phi+} = 0.12$ rad and $\sigma_{\phi-} = 0.08$ rad which, given $\beta_x \sim 20$ m and $\beta_y \sim 20$ m in the vicinity, locates the error to within a few meters. The calculated location for the coupler was at a dipole bend. Upon inspection it was found that the bend had an integrated horizontal steering within it and that the backleg winding of the steering coil had been misinstalled and was next to the beam pipe. That the backleg winding was the source of the coupling was verified by turning off the corrector. No coupling source was seen in the vicinity on a subsequent measurement. The problem was solved by moving the backleg winding away from the beam pipe.

As can be noted from Fig. 4, there are other sources of coupling that can be spotted. For example, from Fig. 4(c) there is an indication of a coupler around detector 94, and Fig. 4(b) shows a coupling source around detector 40. By moving the fit regions around it is possible to locate these additional couplers. Again, like Fig. 3, the plot has been extended by $1/2$ turn to accommodate the analysis when a coupler is near the interaction point (see the discussion in the previous section). In this case, to extend the plot, the necessary equation analogous to Eq. (47) is

$$\overline{C}_{12}(j + 100) = \overline{C}_{12}(j) . \tag{78}$$

## ACKNOWLEDGMENTS

My thanks to Mike Billing for useful discussions, Stu Henderson for providing the phase data, and David Rubin

and Sasha Temnykh for providing the coupling data. Special thanks must go to Robert Meller and Raphael Littauer for their work on the hardware. Thanks also must be made to the other members of the operations group for their support. This work was supported by the National Science Foundation.

## APPENDIX: PROPAGATION OF $\overline{\mathbf{C}}$ IN A COUPLER FREE REGION

In a coupler free region the $4 \times 4$ transfer matrix $\mathbf{T}_{12}$ [not to be confused with the $2 \times 2$ transfer matrix in Eq. (1)] between points $s_1$ and $s_2$ is block diagonal,

$$\mathbf{T}_{12} = \begin{pmatrix} \mathbf{M}_{12} & \mathbf{0} \\ \mathbf{0} & \mathbf{N}_{12} \end{pmatrix}, \tag{A1}$$

where $\mathbf{M}_{12}$ and $\mathbf{N}_{12}$ are $2 \times 2$ matrices. With this, the relationship between $\overline{\mathbf{C}}$ at point $s_1$ and $\overline{\mathbf{C}}$ at point $s_2$ is given by Sagan and Rubin (SR) (Ref. [4], Eq. [35]):

$$\mathbf{C}_2 = \mathbf{M}_{12}\mathbf{C}_1\mathbf{N}_{12}^{-1}. \tag{A2}$$

Note that we do not have to worry about "mode flips" here since mode flips will be forced only if there is a coupler present. The absence of any local couplers also implies that (Ref. [4], Eq. [34])

$$\mathbf{T}_{12} = \mathbf{W}_{12}, \tag{A3}$$

where $\mathbf{W}_{12}$ is defined by SR (Ref. [4], Eq. [23]):

$$\mathbf{U}_2 = \mathbf{W}_{12}\mathbf{U}_1\mathbf{W}_{12}^{-1}, \tag{A4}$$

with $\mathbf{U}$ being defined in Eq. (48). Using Eqs. (49), (A1), and (A3) in Eq. (A4) gives

$$\mathbf{A}_2 = \mathbf{M}_{12}\mathbf{A}_1\mathbf{M}_{12}^{-1} \quad \text{and} \quad \mathbf{B}_2 = \mathbf{N}_{12}\mathbf{B}_1\mathbf{N}_{12}^{-1}. \tag{A5}$$

Equations (A5) show that $\mathbf{M}_{12}$ and $\mathbf{N}_{12}$ connect the normal mode matrices $\mathbf{A}$ and $\mathbf{B}$ between points $s_1$ and $s_2$. As such, they can be written in the form given by Eqs. (2). Using this and Eq. (52) in (A2) gives

$$\overline{\mathbf{C}}_2 = \mathbf{R}(\phi_{a12})\overline{\mathbf{C}}_1\mathbf{R}^{-1}(\phi_{b12}), \tag{A6}$$

where $\mathbf{R}$ is a rotation matrix

$$\mathbf{R}(\theta) \equiv \begin{pmatrix} \cos\theta & \sin\theta \\ -\sin\theta & \cos\theta \end{pmatrix}, \tag{A7}$$

and $\phi_{a12}$ and $\phi_{b12}$ are the phase advances for the $a$ and $b$ modes, respectively. As shown in SR, Appendix A, given any $2 \times 2$ matrix $\mathbf{z}$ there exist numbers $\lambda$, $\kappa$, $\phi$, and $\theta$ such that $\mathbf{z}$ can be written in the form

$$\mathbf{z} = \lambda\mathbf{S}(\phi) + \kappa\mathbf{R}(\theta), \tag{A8}$$

where $\mathbf{S}$ is an "antirotation" matrix of the form

$$\mathbf{S}(\phi) \equiv \begin{pmatrix} \cos\phi & \sin\phi \\ \sin\phi & -\cos\phi \end{pmatrix}. \tag{A9}$$

Using this form for $\overline{\mathbf{C}}(s_1)$ in Eq. (A6), along with the multiplication rules of SR (Ref. [4], Eq. [A11]), shows that in a coupler free region $\overline{\mathbf{C}}$ behaves as

$$\overline{\mathbf{C}}(s) = s\mathbf{S}(\phi_c - \phi_+(s)) + r\mathbf{R}(\theta_c + \phi_-(s)), \tag{A10}$$

where $s$, $\phi_c$, $r$, and $\theta_c$ are constants, and the sum and difference phase advances are

$$\phi_+(s) \equiv \phi_a(s) + \phi_b(s), \qquad \phi_-(s) \equiv \phi_a(s) - \phi_b(s). \tag{A11}$$

[1] D. Sagan, B. Meller, R. Littauer, and D. Rubin, Phys. Rev. ST Accel. Beams **3**, 092801 (2000).
[2] C. Bovet, R. Gouiran, I. Gumowski, and K. H. Reich, CERN Report No. CERN/MPS-SI/Int. DL/70/4, 1970.
[3] W. Press, B. Flannery, S. Teukolsky, and W. Wetterling, *Numerical Recipes in Fortran, the Art of Scientific Computing* (Cambridge University, New York, 1992), 2nd ed.
[4] D. Sagan and D. Rubin, Phys. Rev. ST Accel. Beams **2**, 074001 (1999).